Ocean-sourced snow: An unaccounted process on Arctic sea ice

Amy Macfarlane

amyrmacfarlane@gmail.com

WSL Institute for Snow and Avalanche Research SLF https://orcid.org/0000-0002-1638-8885

Moein Mellat

Alfred Wegener Institute Helmholtz Centre for Polar and Marine Research

Ruzica Dadic

WSL Institute for Snow and Avalanche Research SLF

Hanno Meyer

Alfred Wegener Institute Helmholtz Centre for Polar and Marine Research https://orcid.org/0000-0003-4129-4706

Martin Werner

Alfred Wegener Institute https://orcid.org/0000-0002-6473-0243

Camilla Brunello

Alfred Wegener Institute Helmholtz Centre for Polar and Marine Research

Stefanie Arndt

Alfred Wegener Institute Helmholtz Centre for Polar and Marine Research

Daniela Krampe

Alfred Wegener Institute Helmholtz Centre for Polar and Marine Research

Martin Schneebeli

WSL Institute for Snow and Avalanche Research SLF

Article

Keywords: Sea ice, Arctic, snow, snow metamorphism, temperature gradient, sublimation, isotopes, salinity, biogeochemistry, impurities, mass balance, thermal resistivity, precipitation estimates

Posted Date: November 20th, 2023

DOI: https://doi.org/10.21203/rs.3.rs-3572881/v1

Additional Declarations: There is **NO** Competing Interest.

Ocean-sourced snow: An unaccounted process on Arctic sea ice

Amy R. Macfarlane[1*], Moein Mellat[2], Ruzica Dadic[1,3], Hanno Meyer[2], Martin Werner[4], Camilla F. Brunello[2], Stefanie Arndt[4], Daniela Krampe[4], Martin Schneebeli[1]

[1*]WSL Institute for Snow and Avalanche Research SLF, Flüelastrasse 11, Davos, 7260, Switzerland.
[2]Alfred Wegener Institute Helmholtz Centre for Polar and Marine Research, Telegrafenberg, Potsdam, 14473, Germany.
[3]Victoria University of Wellington, Kelburn Parade, Wellington, 6012, New Zealand.
[4]Alfred Wegener Institute Helmholtz Centre for Polar and Marine Research, Am Handelshafen 12, Bremerhaven, 27570, Germany.

*Corresponding author(s). E-mail(s): amyrmacfarlane@gmail.com;
Contributing authors: moein.mellat@awi.de; ruzica.dadic@slf.ch; hanno.meyer@awi.de; martin.werner@awi.de; camilla.brunello@awi.de; stefanie.arndt@awi.de; daniela.krampe@awi.de; schneebeli@slf.ch;

Abstract

The water isotope composition of the winter snow cover on Arctic sea ice is strongly enriched in heavy isotopes near the snow-sea ice interface, incompatible with typical enrichment values through snow metamorphism processes alone. Our stratigraphic investigations from the MOSAiC expedition, using computed tomography combined with isotopic analyses of the snow, highlight that approximately 20% of the snowpack is not of meteoric origin but created from the sea ice. Here, we show that sea ice sublimation under the high-temperature gradients during the Arctic winter produces a snow-like structure and significantly contributes to the total snow water equivalent on Arctic sea ice. This, until now, unaccounted oceanographic source of "snow" furthers our understanding of i) vapor fluxes and gas exchange through the snowpack with biogeochemistry applications, ii) the formation of saline Arctic snow, and contribution to sea salt aerosols, iii) uncertainties in mass balance and physical properties of snow, and iv) additional uncertainties in precipitation estimates when compared to in situ measurements.

Ultimately, regional differences in precipitation will result in varying local temperature gradients and therefore different contributions of ocean-sourced snow, and understanding this is essential for improving the accuracy of modeled sea ice predictions.

Keywords: Sea ice, Arctic, snow, snow metamorphism, temperature gradient, sublimation, isotopes, salinity, biogeochemistry, impurities, mass balance, thermal resistivity, precipitation estimates

1 Main

As the interfacial layer between the atmosphere and the underlying ice, the Arctic snowpack plays a significant role in atmospheric, sea ice chemical, and physical processes. Snow's insulating properties provide a blanket-like barrier between the sea ice and the atmosphere [1], whilst snow itself is a key element in the mass balance [2] and a source of aerosols [3] and other chemical compounds (e.g bromine [4]). Having accurate estimations of the snow depth and internal processes within the snow cover on Arctic sea ice is critical for many components of the sea ice system [1] and essential for our predictions of sea ice thickness in this delicate region [5]. However, despite snow's importance in the Arctic sea ice system, we fail to explain how internal snow physical processes impact the salinity and isotopic composition of the snow cover and the effects of the snow's physical properties on the regional Arctic sea ice system.

1.1 Snow temperature gradient metamorphism

Temperature gradient metamorphism (TGM) occurs in snow due to internal temperature gradients, driving the movement of vapor from warmer to colder regions within the snow cover [6]. This leads to snow re-crystallization through vapor sublimation and deposition within the snowpack. These internal vapor fluxes will likely alter the isotopic signature of the snowpack [7, 8]. We calculate the temperature gradients using equation $\Delta T_z = (T_i – T_s)/h_s$, where the snow-sea ice and snow-atmosphere interface temperatures (T_i and T_s) and snow height (h_s) are annotated in Figures 1a and 1c.

In laboratory experiments testing extreme temperature gradients on snow metamorphism, the snowpack has been observed to undergo significant structural transformations. A study [9] applied a 103 K m^{-1} gradient across 7.7 cm of rounded-grained snow, resulting in a 3 mm air gap forming at the base of the snow after 28 days. Another investigation [10] measured microstructural changes of a snowpack above an ice lens after applying a 100 K m^{-1} gradient for 21 days. Sublimation caused the ice lens to move downward. Figure 1a shows a modified micro-computer tomography image from this study [10], and illustrates the effects of sublimation on an underlying ice surface and the snow microstructure. These laboratory findings were tested through simulations of vapor fluxes under a known temperature gradient using the SNOWPACK model [11], which found a density decrease at the sea ice-snow interface by –20 % while there is a deposition layer above it with a 5 % increase in density.

Stable water isotopes (δ^2H and δ^{18}O) are geochemical tracers, elucidating the historical trajectory of snow, spanning vapor origins, re-crystallization, transport and conditions [12]. A winter snowpack is composed of the solid and vapor phases of water, and any phase transition can lead to fractionation processes (the preferential partitioning of heavier and lighter isotopes), leading to changes in the isotopic composition of the snowpack [13]. As a result, isotopic profiles provide insights into these post-depositional processes occurring within the snowpack [14]. The ratio of the heavier to lighter water isotopologues, δ^2H and δ^{18}O, are given as the deviation from Vienna Standard Mean Ocean Water (VSMOW), expressed in per mil (‰).

In our study, we investigate post-depositional TGM effects on Arctic snow from January to May 2020 (therefore excluding melt influences) during the MOSAiC expedition. Through in-situ measurements, we analyze TGM's impact on snow isotopic composition, physical properties, and snowpack mineral precipitation (Sections 1.2.1 to 1.2.3). The snowpack exhibited an average temperature gradient of 52 $\pm$ 51 K m^{-1} (Figure 2c), aligning with laboratory research [9, 10]. By integrating in-situ data with laboratory experiments, we enhance our understanding of how TGM affects the geochemical and physical traits of snow on Arctic sea ice.

1.2 Results

1.2.1 Stable water isotopes as tracers

TGM can homogenize the entire snowpack's isotopic signature, reducing the composition variability over time [13]. Mass losses (caused by evaporation and sublimation) preferentially enrich the snow in the heavy isotope ^{18}O, and mass gain (due to condensation and deposition) preferentially enrich snow in light-isotopes (depleting ^{18}O) [15].

[16] conducted a 9-year experiment investigating the influence of TGM on the isotopic signature of a snowpack. Over the course of a season (150–200 days), they found the basal soil-pack sample (0–10 cm) of the snowpit site at Fairbanks showed enrichment in the heavy isotopes (e.g., ^{18}O by 3.3 ‰). The sublimated material, depleted in heavy isotopes, was incorporated in the snow immediately above this bottom portion of the soil pack (the 10–20 cm layer). We roughly represent the δ^{18}O isotopic profile as T2 in Figure 1b, with a 15 % variation from the original isotopic signal (see the true profile in Appendix A2). The snowpack with temperature gradients was compared to a snowpack deposited on a nearby wooden table, not subjected to a thermal gradient, idealized as T1 in Figure 1b.

Despite the snow isotopic profile's high variability (explained in Appendix B), we found the average snow sample at the snow-sea ice interface is substantially more enriched in δ^{18}O than a surface snow sample (Figure 2a). The negative covariance in Figure 2a (–62.25 ‰-cm) suggests a negative association between the sample height in the snowpit and δ^{18}O. In this manuscript, we explain this association and relate this to the extreme sublimation of the lower snowpack and underlying sea ice [9, 10].

We expect fresh snow precipitation in the upper layers and snow that has undergone TGM to have distinguishable isotopic signals. However, after investigating the second-order isotope parameter, deuterium excess (d-excess = δ^2H $-8 \times \delta^{18}$O) [12], which is

specifically sensitive to the conditions during sublimation [17], we measured negative values (between snow height 0–5 cm, the average d-excess is –1.2 ± 10.5 ‰ with a minimum d-excess of –26.6 ‰). Meteoric snow typically has positive d-excess values, and sea ice in contact with the snow has d-excess values close to 0 ± 4 ‰. D-excess depends mainly on temperature and humidity during primary evaporation at the moisture source [17], and changes in d-excess are driven by non-equilibrium fractionation processes during sublimation and re-sublimation within the already deposited snowpack. [12].

Figure 2 shows how snow TGM triggers sublimation in the underlying sea ice, driving a substantial transition in the δ^{18}O and d-excess signals of the Arctic sea ice snowpack. The significantly negative d-excess values stem from complex metamorphic sublimation processes at the snow-sea ice interface. These lead to disproportionate fractionation of δ^{2}H and δ^{18}O and result in the negative d-excess values observed at the snow-sea ice interface. Using a water vapor-saturated airflow [8] and [18] showed strong changes in snow isotopic composition, where one experiment showed the vapor ($\Delta\delta^{18}$O= 55 ‰) significantly change the original δ^{18}O isotope signal in the snow by up to 15 ‰ in 84 hours. This supports our hypothesis that the vapor from the sublimating sea ice deposits in the snowpack, and significantly contributes to snow mass. We show this hypothesis as a theoretical profile, labeled T3, in Figure 1b.

1.2.2 Microstructural parameters as tracers

The co-located measurements of isotopic composition and physical properties (see Section 2 for details) help advance our understanding of internal post-depositional processes within the snowpack on Arctic sea ice. The higher specific surface area (SSA) values of >15 m^2 kg^{-1} (cross markers in Figure 3) above a snow depth (h) of 15 cm likely correspond to freshly precipitated snow samples, these are also the samples with the most depleted δ^{18}O signals, likely corresponding to a meteoric snowfall signal.

In Figure 3a, the bottom 0–5 cm of the snowpack have samples with a $\rho > 550$ Kg m^{-3} and an enriched δ^{18}O signal. These are high-density samples collected at the snow-sea ice interface, likely resulting from different formation processes (e.g., flooding causing a snow-ice layer or a remnant surface scattering layer from the previous melt season [19], see section B). After we exclude these samples, many samples remain ($\rho < 550$ Kg m^{-3}) with extremely enriched δ^{18}O at the snow-sea ice interface. We do not see a significant reduction in density in the lower layers of the snowpack, contrasting to the measured density decrease in [9] and [11]. This could result from our underlying ice layer replenishing the sublimating snow crystals. [6] observed a mass turnover of up to 60 % of the total ice mass per day, leading to a typical lifetime of the ice crystals on the order of 2–3 days under a temperature gradient of 50 K m^{-1}. We hypothesize that our "snow" ($\rho < 550$ Kg m^{-3}) located at the bottom of the snowpack is substantially more metamorphosed than initially expected and that it is composed of re-deposited ocean-sourced vapor originating from the underlying sea ice.

Anisotropy has an average value of 1.13 (unitless) with a standard deviation of 0.06 (Figure 3c). Anisotropy >1 represents vertically aligned structures, and <1 are horizontally aligned structures. Our anisotropy values in Figure 3c show that the majority of samples are vertically aligned and have likely undergone TGM. The grain

types at the lower layers in the snow Arctic sea ice were observed as mostly depth hoar crystals, and a cross-section of the typical depth hoar structure (a known product of TGM) can be seen in Figure 4d.

1.2.3 Shedding light on snowpack salinity

Currently, saline snow on Arctic sea ice is hypothesized to be a result of sea spray (containing dissolved salts) being incorporated as a result of wind [20], brine wicking (the movement of brine by capillary action) of liquid brine on a re-frozen lead [21], and through processes involving saline frost flowers; incorporation when snow falls on top [22] and re-distribution of frost flowers by wind [20] (see Figure 1c). In Figure 4c, snow samples collected on level ice, melted, and measured for salinity are depicted. Samples with higher salinities are found near the sea-ice interface.

We compared our snow samples' d-excess and salinity values and highlighted two independent features. Firstly, saline samples with a positive d-excess occur in samples collected on snow above refrozen leads (see Figure 4a), likely a result of wind-blown snow accumulating on the leads, which has not undergone substantial TGM or isotopic fractionation, but has experienced brine wicking causing the high salinity. Secondly, examining Figure 4a, it becomes apparent that the majority of salinity samples collected on level ice exhibit negative d-excess values. This phenomenon cannot be attributed to sea spray, brine wicking, or frost flower inclusion processes, as these mechanisms typically do not result in decreasing d-excess values. Instead, our findings suggest that the occurrence of negative d-excess values in the saline snowpack, in combination with enrichment of snow in heavy isotopes at the interface, can be linked to sublimation of the underlying sea ice surface, characterized by non-equilibrium fractionation. Samples taken from level (first-year ice and second-year ice; FYI and SYI) ice contain the vast majority of the samples with negative d-excess values (Figure 4b), relative to the snow samples taken from re-frozen lead and ridged ice. This could be a result of the consistently higher temperature gradients in the stable snowpack on level ice, resulting in more intense TGM and sublimation of the sea ice. We see a greater contribution of ocean-sourced "snow" on level ice in contrast to the atmospheric-sourced snow on leads, which has had smaller temperature gradients.

Through x-ray computer tomography, we observed highly reflective, saline pockets (precipitated minerals within the snow cover [23], Figure 4d). During this winter study period, the snow-sea ice interface temperature was, on average, –13.3 ± 4.2 ^{o}C. Salt does not sublimate at these low temperatures but undergoes crystallization under high concentrations, producing different hydrated salts [23]. Unfortunately, we did not test for precipitated minerals, but only for the conductivity of the melted snow (melting dissolves these minerals), and found that 58 % of the samples had a salinity greater than zero (Figure 4a). These highly reflective pockets were located within the snow structure and not in the intergranular spaces (as would be the case with capillary action). We hypothesize that sea ice sublimation creates a porous snow-like structure, and minerals remain in the residue in pockets within the microstructure when the surrounding ice sublimates. As a result, snow salinity indicates the presence of ocean-sourced "snow" on level ice areas.

1.2.4 Quantifying the SWE contribution of ocean-sourced "snow"

a) Snow sublimation rate, based on [9]'s empirical study. This study saw 3 mm of snow sublimate in 21 days (0.143 mm d^{-1}), when the experiment had a 103 K m^{-1} temperature gradient with -6.5 °C at the snow base and –14.5°C at the snow surface. Over 150 days, this gives 21.4 mm (150 d × 0.143 mm d^{-1}) of sublimated snow depth equivalent, equating to snow water equivalent (SWE) of 6.3 mm (assuming a snow density of 300 kg m^{-3}).
b) Sublimation rates of an ice surface, based on the linear fit of the ice lens surface movement from [10] provided in Equation C1 contributes to a snow depth equivalent of 51.25 mm (corresponding to a SWE of 15.4 mm) when the snow was –3 °C and the air temperature was between –11 and –16 °C. Further details on this calculation are provided in Appendix C.
c) Isotope analysis resulted in 21 ± 1 % of the precipitated signal originating from the underlying sea ice sublimation and deposition. This is a SWE of 13.44 mm (see Appendix C.2 for details). However, this calculation neglects snow fractionation processes during metamorphism, which enrich the snow in heavy isotopes, likely causing an ocean-sourced SWE overestimation.

1.3 Discussion

Modeling snow TGM and vapor fluxes. Adding a sublimating sea ice surface as an additional vapor source contributes mass to the base of the snowpack and counteracts the SNOWPACK modeled density reductions [11]. Additionally, including vapor fluxes through the snow is necessary for modeling gas exchanges through the Arctic sea ice and snow and has a detrimental effect on our understanding of sea salt aerosol sources and their role in polar climate [24].

Gas fluxes essential for biogeochemistry applications. Transmission of gases through the snowpack dominates the local chemistry of the lower atmosphere and is responsible for the depletion of tropospheric ozone and gaseous mercury [25–27]. We expect to see increased diffusivity if ice is substituted by a porous snow layer. The source of vapor and the corresponding isotopic signature of the snowpack could be used as tracers of gas diffusion within the snowpack, e.g., nitrogen oxides, sulfur dioxide, and atmospheric aerosols. In addition to constraining a possible source of bromine and molecular iodine in the Arctic sea ice system contributing to Arctic ozone destruction [27].

Distribution of snowpack impurities. Extreme sublimation and deposition within the snow and on the snow surface are critical for exchanging chemical species with the atmosphere and potentially heavily influence the deposition and uptake of atmospheric pollutants. Black carbon studies emphasize that extreme sublimation implies that snow mass is lost while impurities remain, and sublimation and freezing within the snowpack are likely to expose internal black carbon [28]. Impurities are easier to be released from the snowpack than from the ice during a wind-blowing event, and there is evidence that sea-salt aerosols from blowing snow events contribute to Arctic warming [3].

Mass balance and thermal resistance. The creation of "snow" at the snow-ice interface increases the depth and thermal resistance of the snow cover. This process needs equivalent attention to that given to flooding (and snow-ice formation) on Antarctic sea ice, which loses snow mass (0.1–0.4 m [29]). Typical depths of the Arctic sea ice snowpack measured during MOSAiC are 130 ± 99 mm. An introduction of 50–54 mm of ocean-sourced snow is a significant source of uncertainty when modeling the mass balance of sea ice. This process transforms a highly conductive material (ice with thermal conductivity of 2.34 W K^{-1} m^{-1}) into a low conductivity material (snow with thermal conductivity of 0.27 ± 0.17 W K^{-1} m^{-1}; [30]). Adding 51.25 mm to the snow depth increases the snow's thermal resistance by 0.19 K m^2 W^{-1} (35 % relative to snow thermal resistance on the level sea ice; 0.54 K m^2 W^{-1}). This has significant consequences when calculating ice growth rates, and this new source of snow is not yet accounted for in any process models.

Precipitation estimates. When precipitation is modeled throughout the Arctic, we often compare it to in situ snow water equivalent measurements for validation [31]. If 2–5 cm of the snow on sea ice is from the sublimation of the sea ice surface, we are underestimating the snow water equivalent of snow on Arctic sea ice if measuring remotely (e.g., reanalysis precipitation estimates). This has major implications on our estimations of snow mass and redistribution of the snow in the Arctic, which in turn, introduces uncertainties in the amount of snow deposited into leads and accumulating around ridges, further influencing calculations of Arctic heat flux.

Arctic snow and sea ice in a future climate. Arctic climatic predictions point towards substantial regional differences in precipitation [32]. A thicker snowpack would result in smaller temperature gradients, meaning less metamorphism, and less ocean-sourced snow at the interface. However, a higher risk of flooding and snow-ice formation. More work is needed to understand post-depositional processes on sea ice, and the interaction with flooding processes. In contrast to this, less snow accumulation would result in a shallower snowpack with higher temperature gradients, more metamorphism, more isotope enrichment in the heavy isotopes, and a higher contribution of ocean-sourced snow. Finally, the reduction in multi-year ice extent and thickness [33] and the strong correlation between the average salinity and the ice thickness could result in an Arctic ice cover with higher salinity, resulting in a more saline (precipitated minerals) snow cover.

2 Online methods

2.1 In-situ observations

This manuscript studies snow on sea ice in the winter months from January 2020 to May 2020 in the high Arctic between 83.4^{o}N and 88.6^{o}N. The research vessel (RV) Polarstern was drifting alongside a single ice floe as part of the MOSAiC expedition. To describe the evolution of the snowpack conditions over time, we set up "snowpit sites" on the ice floe. We built a time series of the snowpack's physical, (isotope) geochemical, and salinity development by repeatedly visiting the same measurement locations. We returned to these snowpit sites weekly unless ice dynamics meant they

were inaccessible. The snowpit sites included level ice areas, leads, and ridges. The set-up of these snowpit sites on the ice allowed for in-situ measurements of snow properties [34]. Designated areas were assigned to snow measurements on the MOSAiC winter floe and named "snowpits". The snowpit sites were chosen randomly and were a collection of measurements taken within one "event". One event includes a library of different snow measurements measured simultaneously during one trip to the ice [35]. The snowpit research used in this manuscript focuses on microstructural and chemical analysis of snow, including salinity and stable water isotope measurements. More details on the data collection methods can be found in the datapaper [36].

Snow microstructural measurements were taken within the snowpits alongside the isotope and salinity profiles. A desktop cone-beam microCT90 (microCT) installed in a laboratory onboard the RV [37] provides us with the microstructural information of the snowpack at one location and one point in time. Analysis with the microCT requires snow samples to be collected in the field, transported to the Polarstern, and measured using the microCT. A threshold of 0.21 was selected to separate the ice and air volumes to obtain profiles of density, SSA, and geometric anisotropy. This threshold remained constant throughout the season and was tested using monthly reference scans of targets of known density. These profiles are publicly accessible on Pangaea [37].

2.2 Isotopic analysis

Within the snowpits, isotope samples were collected in vertical profiles. Snow samples were taken in the field and analyzed after returning to onshore laboratories. In total, 514 isotope samples were collected and analyzed in two laboratories (The Swiss Federal Research Institute WSL and the ISOLAB Facility at the Alfred Wegener Institute Helmholtz Centre for Polar and Marine Research in Potsdam, Germany) for the study period between January and May 2020. Both datasets contribute to this manuscript. The first dataset [38] took vertical profiles of snow samples (each 100 cm^3). These samples were measured for density in the field and then transported to the ship in sealed plastic cups. The vertical resolution of these samples was every 3 cm. After the samples were transported to RV Polarstern, the samples were melted for salinity measurements (using the YSI 30 Salinity, Conductivity and Temperature sensor, [39]) and sealed into glass jars onboard Polarstern. As a result of this sampling protocol, $\delta^{18}O$ and $\delta^{2}H$ were measured at the same intervals as the density and salinity profiles. Each sample in this dataset was transported to Switzerland and measured for stable water isotopic composition at WSL, Zurich, using a Los Gatos Research (LGR) Isotopic Water Analyzer (model IWA-45EP) instrument. Each sample was measured five times in this dataset [38] with a resulting measurement uncertainty of $\delta^{18}O \pm 1$ ‰ and $\delta^{2}H \pm 2$ ‰, and accuracy of $\delta^{18}O \pm 0.5$ ‰ and $\delta^{2}H \pm 1$ ‰.

A second dataset was collected in the snowpit at three layers: top, middle, and bottom. A plastic shovel was used to sample the snow in these three layers directly into plastic bags. These samples were transported to RV Polarstern and remained frozen onboard as they were stored at -4^{o}C. After the expedition, this second dataset was sent to AWI, Germany, thawed at room temperature, poured into 20 ml glass vials, sealed with parafilm tape, and stored at 4°C. This dataset was measured for stable

water isotopes using mass spectrometers (DELTA-S Finnigan MAT, USA) using equilibration techniques to an accuracy of ∼0.1 ‰ for δ^{18}O and ∼0.8 ‰ for δ^{2}H. Every sample is equilibrated and then transferred to the IRMS, where it is measured 10 times against a standard of known isotope composition. The statistics of one single datapoint is based on these ten measurements. Both datasets are published with open access in Pangaea, where more details can be found. A comparison was conducted between the two laboratories by measuring 50 samples twice to show continuity between the datasets. It was found that the WSL-measured samples needed a correction due to evaporative fractionation during sample storage. The correction was done by calculating the mean of this dataset to the mean of the parallel dataset from AWI and correcting for the difference. This was possible as the histograms for both datasets were of a similar shape but appeared to have a shift. For details, see PANGAEA. As a result, the δ^{18}O was corrected by –6.4 ‰, the δ^{2}H was corrected by –36.4 ‰.

3 Figures and tables

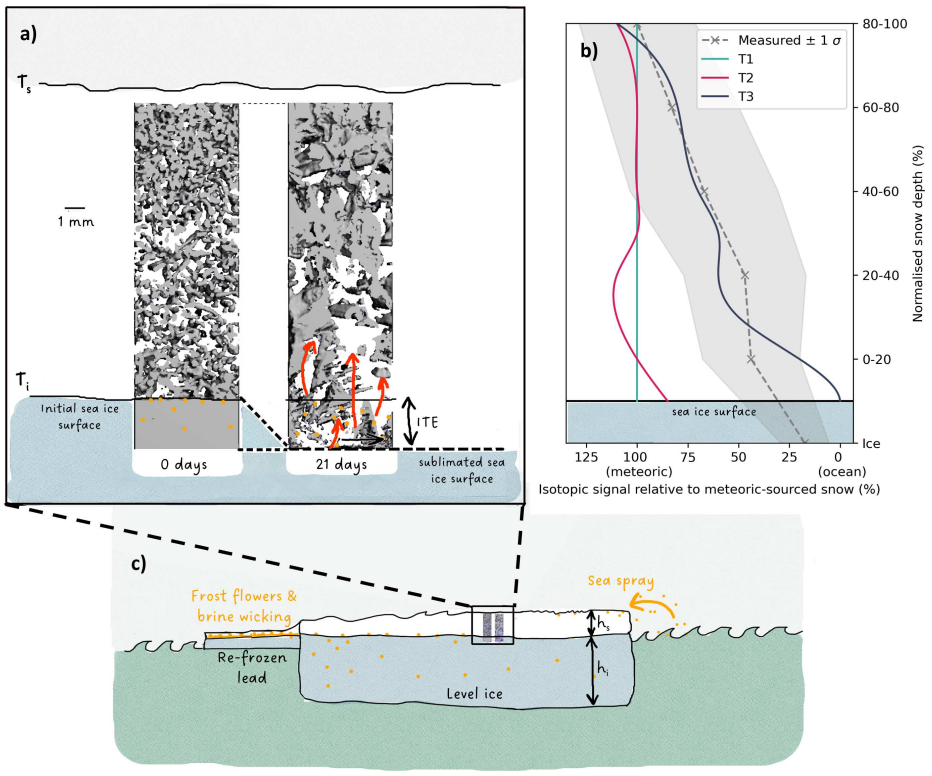

Fig. 1: A schematic with a) a micro-computer tomography image overlayed, adapted from [10], to illustrate the sublimation of the snow-sea ice interface over 21 days. The red arrows represent vapor fluxes from the sea ice surface and the deposition and formation of depth hoar crystals. ITE represents the height of sublimation of the sea ice surface (named ice thickness equivalent in this study). The scale bar represents 1 mm. T_s and T_i are the temperatures of the snow and ice surface, respectively. b) shows the normalized average isotopic snow profile measured in this study (labeled "Measured") relative to the meteoric-sourced snow $\delta^{18}O$ at the surface with standard deviations ($\pm 1\sigma$) shown as the shaded area. T1 is a theoretical profile that has not experienced temperature gradient metamorphism or an underlying sea-ice source, and T2 is a theoretical profile experiencing temperature gradient metamorphism but without an underlying sea-ice source. T3 is the theoretical profile experiencing temperature gradient metamorphism with an underlying sea-ice source. c) shows a cross-section of the Arctic sea ice system (adapted from [20]), where the orange represents typical locations of precipitated minerals, h_s is the snow height, h_i is the ice thickness. This background schematic is not drawn to scale.

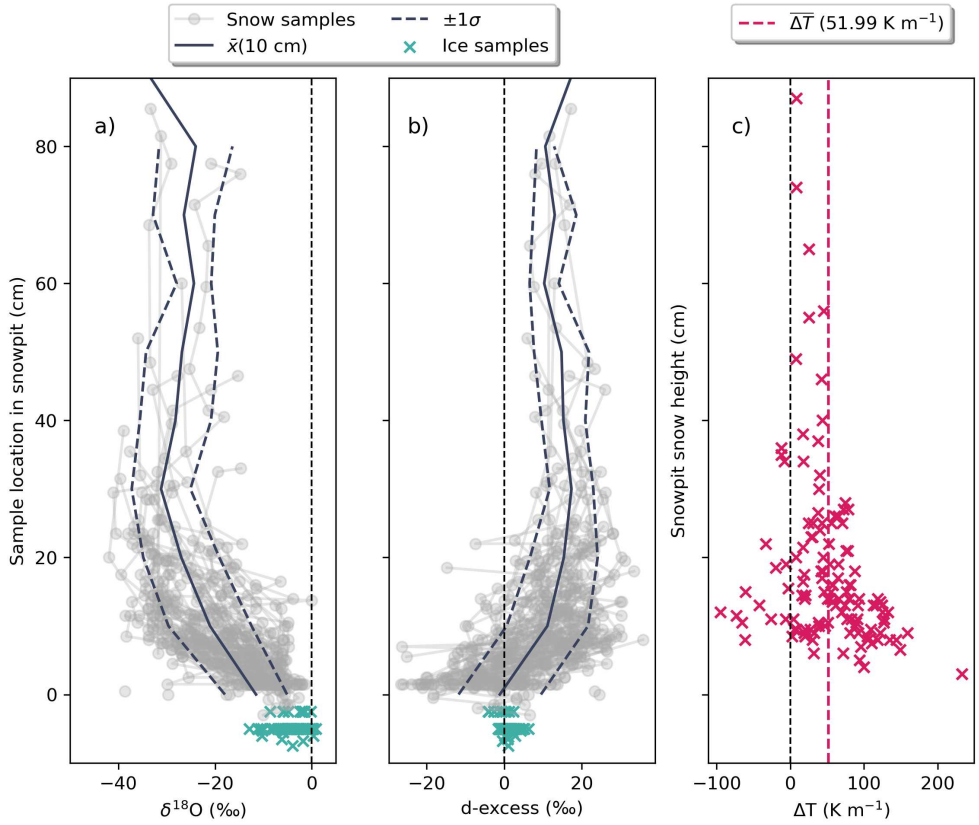

Fig. 2: The snowpack's winter vertical profiles of a) δ^{18}O, b) d-excess, where one grey point represents one sample collected in a snow profile during winter (January - May 2020), the solid line indicates the vertically averaged 10 cm mean, and the dotted lines indicate one standard deviation ($\pm 1\sigma$). Sample location in snowpit = 0 cm represents the snow-sea ice interface. Samples located above 30 cm are taken in snowpits at ridged locations with high snow accumulation. c) The measured temperature gradients plotted against snowpit snow height for each snow profile measured in this study period between January and May 2020. The temperature gradient is positive when the sea ice surface temperature (T_i) > snow surface temperature (T_s). One point represents one snow profile.

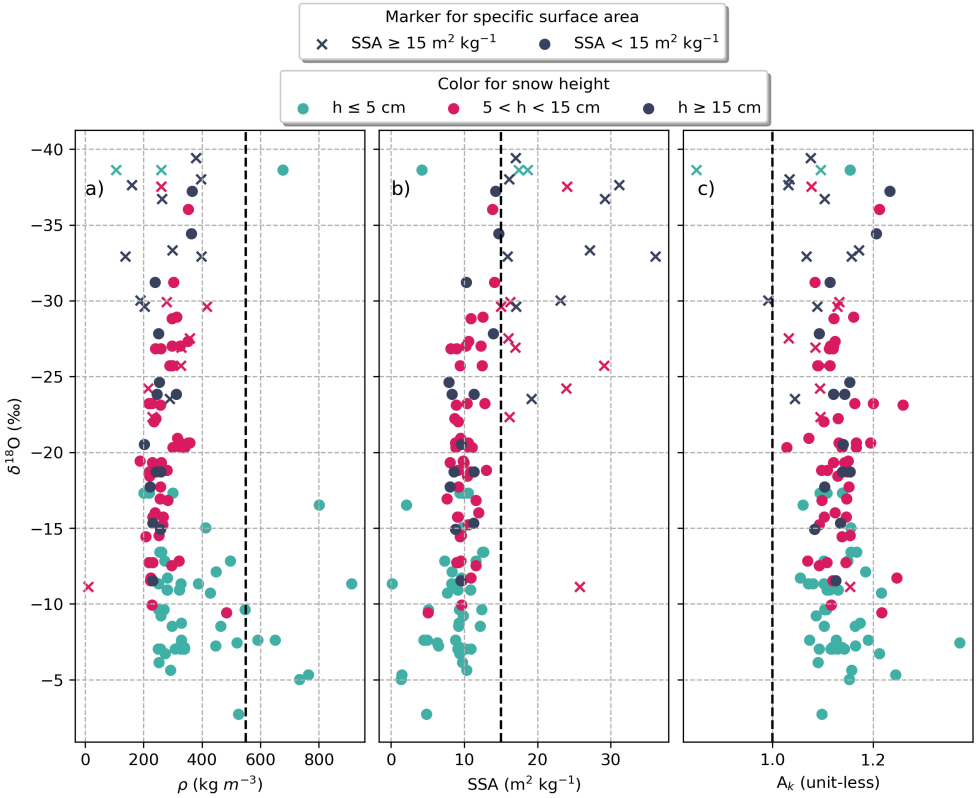

Fig. 3: Co-located micro-computer tomography samples and isotope samples provide the unique simultaneous analysis of chemical and microstructural properties of the snow on Arctic sea ice. The oxygen-18 to oxygen-16 ratio (δ^{18}O) is plotted against a) the snow density (ρ), with a dotted line to show the 550 kg m^{-3} threshold separating snow and high-density interface samples, b) the specific surface area (SSA), with a dotted line to show the 15 m^2 kg^{-1} new snow threshold, and c) the snow's degree of geometric anisotropy (triangulation based, A_k), with a dotted line to show the samples above and below the anisotropy of 1. The marker types are defined by the specific surface area (SSA), and the color of the markers is defined by the height the sample is collected in the snowpit (h) indicated in the legend.

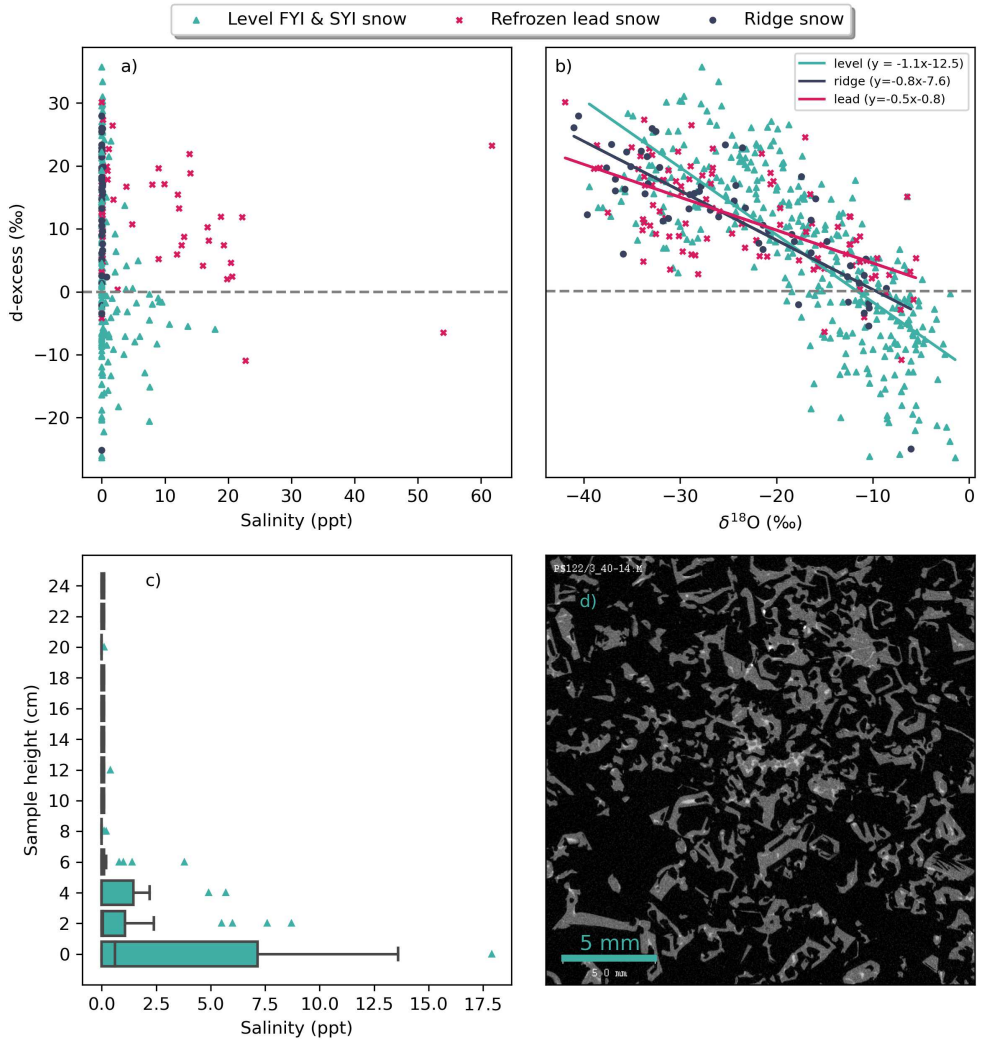

Fig. 4: a) δ^{18}O against deuterium-excess. b) Sample salinity values against deuterium excess. The colors in both plots indicate the underlying ice type: level ice, refrozen lead (Lead) or ridge. Each marker in this figure is one snow sample. The sample collection period is between January and May 2020. c) The salinity box plot profiles of all snow samples collected on level ice, showing the relatively high salinities at the snow close to the snow-sea ice interface. d) A cross-section of a micro-computer tomography scan of snow on Arctic sea ice showing the highly conductive pockets in a bright white, the depth-hoar snow structure in grey, and the air in black. The bright white areas can be interpreted as precipitated minerals within the snow structure. The scale bar on the bottom left represents 5 mm.

Declarations

Acknowledgments

We would like to acknowledge the time spent and the care taken by the AWI and WSL laboratories when conducting the stable water isotopic analysis of all the snow and ice samples. Datasets used in this manuscript were produced as part of the international Multidisciplinary drifting Observatory for the Study of the Arctic Climate (MOSAiC) with the tag MOSAiC20192020 and the Project_ID: AWI_PS122_00. We thank all the people involved in the expedition of the Research Vessel Polarstern during MOSAiC in 2019–2020 as listed at https://doi.org/10.5281/zenodo.5541624. We would like to thank Scanco Medical AG for lending and supporting the use of the Micro-CT90 throughout the MOSAiC expedition.

Funding

This work was possible due to the funding received by:
Swiss Polar Institute (SPI reference DIRCR-2018-003) Funder ID: http://dx.doi.org/10.13039/501100015594.
European Union's Horizon 2020 research and innovation program projects ARICE (grant 730965) for berth fees associated with the participation of the DEARice project.
WSL Institute for Snow and Avalanche Research SLF. WSL_201812N1678. Funder ID: http://dx.doi.org/10.13039/501100015742.
SA received funding through the German Research Foundation's (DFG) projects fAntasie (AR1236/3-1) and SnowCast (AR1236/1-1) within its priority program "Antarctic Research with comparative investigations in the Arctic ice areas" (SPP1158), the DFG Emmy Noether Programme project SNOWflAke (project number 493362232), and the Alfred-Wegener-Institut, Helmholtz-Zentrum für Polar- und Meeresforschung.

Competing interests

The authors declare that they have no known competing interests.

Ethics approval

Not applicable

Consent to participate

Not applicable

Consent for publication

Not applicable

Availability of data and materials

All data is available to download from Pangaea through the following links : snowpit data [35], the first isotope dataset measured at WSL [38], the second isotope dataset measured at AWI [40]. Snow height data measured in the snowpits is available at [41]

Code availability

Not applicable

Authors' contributions

A.R.M and M.M devised the study. A.R.M managed the research, conducted the investigation and wrote the original draft. A.R.M., M.M, H.M, C.F.B, M.W, R.D, and M.S processed the data. M.S. acquired the funding. A.R.M, S.A, D.K., and M.S were data curators. All authors revised and improved the manuscript.

Appendix A Dataset overview

An overview of the isotopic data can be found in Figure A1. As mentioned in the methods, one of the isotopic dataset corrections needed to be corrected. The difference between these two corrections is 5.7‰. As a result of this, the correction produces a d-excess shift. This needs prudent interpretation, especially of the corrected d-excess. Despite this, the uncorrected dataset still has the negative d-excess values and showed the same distribution in the profile, as shown in the original data set publication [40]. Numerous studies show $\delta^{18}O$ values influenced by internal snow processes [42–44]. However, our study is unique as we have an underlying sea ice vapor source enriching the snowpack in ^{18}O. The theoretical profiles seen in Figure 1b (labeled T2 and T3) show the differences between isotopic snow profiles on permafrost and with a sea ice substrate. The true isotopic values used to create the T2 profile in Figure 1b are provided in Figure A2 from [16].

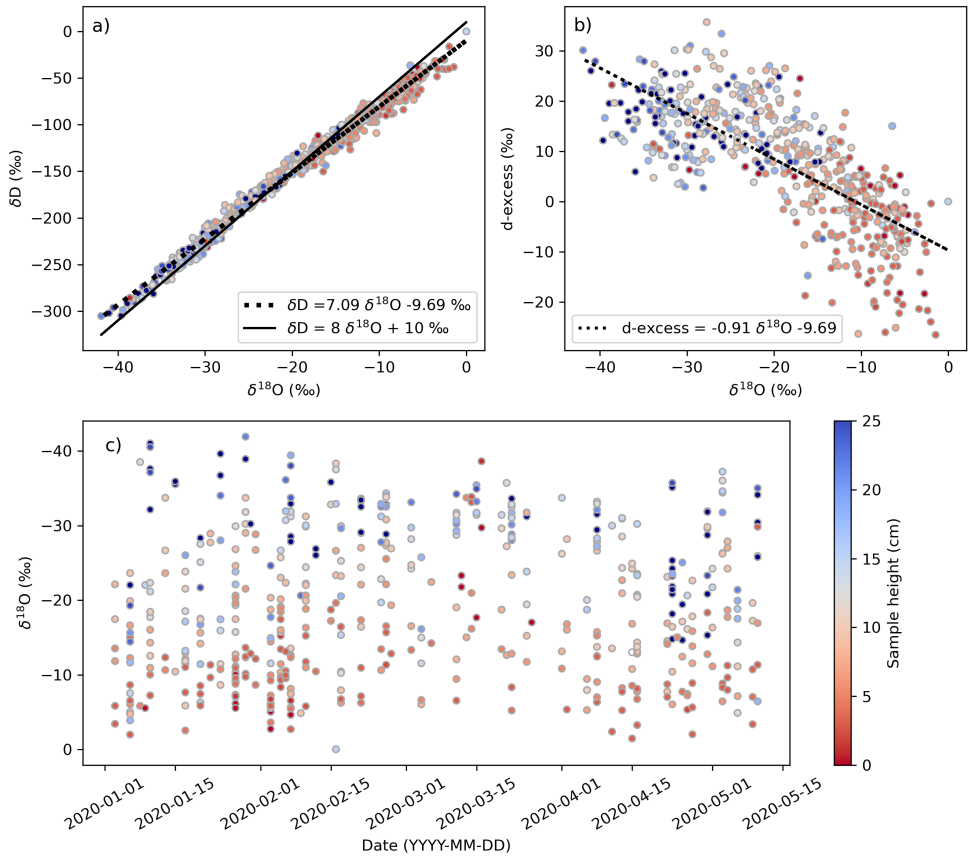

Fig. A1: Stable water isotope analysis for the snow samples collected within the snowpits on the MOSAiC expedition a) the δ^{18}O δ^{2}H co-isotope plot, b) the δ^{18}O against d-excess, and c) time series of δ^{18}O. In all three plots, color represents the height of the top of the sample from the sea ice surface. The navy points represent samples collected above 0.25 m snow height, indicating samples collected at ridged ice areas.

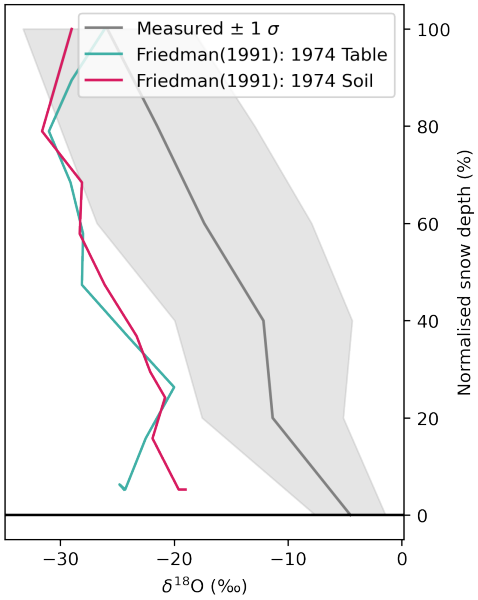

Fig. A2: The true profiles which were used to create the theoretical profiles T2 in Figure 1. The values used in this are the normalized profiles from the year 1974 from two co-located profiles, one on a table (without a temperature gradient) and one on soil (experiencing a temperature gradient throughout the season) from [16].

Appendix B Stratigraphic variability in the Arctic snowpack

The isotope profiles measured in this manuscript highlight the complexity of the snow in the sea-ice system through their high isotopic variability. Stratigraphy of the snow cover on Arctic sea ice is typically modeled and considered a two-layered medium with a wind slab with an underlying depth hoar layer. However, [36] explains the complexity of the snowpack stratigraphy and we now understand how each profile is physically unique in its distribution. This may simultaneously produce large variability within the isotope profiles. An initial plot of all the profiles taken throughout the MOSAiC expedition is visualized in Figure 2, where we can see the averaged profile and the profile's standard deviation. The average standard deviation for the entire profile is 6.7 ‰.

In the manuscript, we briefly mention higher-density snow samples at the sea-ice interface (ρ >550 Kg m^{-3}) with an enriched δ^{18}O signal (seen in Figure 3a). We explain that these could be a result of flooding causing a snow-ice layer or a remnant surface scattering layer from the previous melt season. Flooding of the sea ice surface is caused by the weight of the overlying snow submerging the sea ice surface below the ocean surface, causing a negative freeboard. This is typically a process seen in Antarctica due to higher precipitation rates in this region. However, flooding has been

recorded close to the marginal ice zone in the Arctic during the 2015 N-ICE cruise [45], resulting in snow-ice formation (additionally, forcing this is a suggested response to future warming scenarios [46]). This process would introduce a highly saline icy layer at the snow-sea ice interface, with a $\delta^{18}O$ signal of 0 ‰ and a density close to ice $\sim$ 900 Kg m^{-3}. By investigating the microstructure through micro-CT measurements, and excluding measurements above 550 Kg m^{-3}, we find density values in the range typically classified as "snow" (100 – 550 Kg m^{-3}) with a high isotopic enrichment in the heavy isotopes. As a result, flooding (and a snow-ice layer at the snow-sea ice interface) does not influence our results or discredit the formation of ocean-sourced snow.

In addition, a remnant surface scattering layer may also be present at the snow-sea ice interface on multi-year ice. This is a result of the highly-porous melting sea ice surface layer [19] persisting from the previous melt season and then being covered by a layer of snow at the beginning of Autumn [47]. When this layer is present at the snow-sea ice interface, it ranges from 1 – 2 cm in penetrable depth with ρ <550 Kg m^{-3}. Therefore, excluding high-density samples in Figure 3a and still having isotopically enriched values above 2 cm into the snowpack shows the secondary process of sea ice sublimation having an effect on the isotopic profile.

Appendix C The rate of the sea ice sublimation

C.1 Comparisons to controlled laboratory conditions

Here we outline the similarities and differences between the in-situ measured vapor flux and the controlled laboratory conditions in [10] and provide details on the calculations of the sublimated ITE values.

[10] applied a 100 K m^{-1} temperature gradient to a snow sample (with a surface temperature between –11 and –16°C and a base temperature of –3 °C over a snow sample of height 100 mm), with a higher temperature at the bottom for (with the snow density, ρ_s = 201 kg m^{-3} and SSA = 15.4 m^2 kg^{-3}) on top of an ice lens with a height of up to 16 mm. This snow density is marginally lower than the conditions found on sea ice in the Arctic [30]. However, a temperature gradient of 100 K m^{-1} was not uncommon in our study region (Figure 2c), with an average temperature gradient of 52 ± 51 K m^{-1}. [10] calculated the apparent movement of the ice lens from the ice-voxel fraction profile (where the ice-voxel fraction was equal to 1 in the ice lens).

The linear fit of the ice lens surface movement from [10] is given in Equation C1, where t corresponds to the time in days, and $z_{il} - z_{il,0}$ represents the height of sublimation of the sea ice surface (named ice thickness equivalent, ITE, in this study).

$$z_{il} - z_{il,0} = 0.11 \times t + 0.07 \tag{C1}$$

Sublimation of the ice surface between January and May 2020 (150 days) has an ITE of 16.57 mm. ITE can be converted to equivalent snow depth (SDE) by taking the average density of snow and ice as ρ_s = 291 kg m^{-3} (from average density snow micro-penetrometer measurements in [30]), and ρ_i = 900 kg m^{-3}, respectively, and then applying Equation C2. This results in a snow depth equivalent, SDE = 51.25

mm, using this method.

$$SDE = ITE \times \frac{\rho_i}{\rho_s} \tag{C2}$$

[10] also concluded that the rate of ice mass flux (j_a) from the sublimating ice lens into the snow was $j_a = v_i \rho_i = 1.2{\times}10^{-6}$ kg m^{2}s^{-1}, where v_i is the rate that the ice lens sublimated. In 150 days this amounts to 15.55 kg m^2 of sublimated ice mass.

C.2 Isotope composition when mixing two mediums

The proportion of δ^{18}O in a mixed water or ice body is directly proportional to the original concentration of the water bodies. In a two-component mixture, the contribution of each source can be directly calculated if the initial concentration of δ^{18}O in the two bodies is known [13], seen in Equation C3, where s1 and s2 represent the two isotopic sources: oceanographic and meteoric respectively.

$$\delta^{18}O_{\text{mixed}} = \text{a}\ \delta^{18}O_{\text{s1}} + b\ \delta^{18}O_{\text{s2}} \tag{C3}$$

In the sea ice environment, we have a clear differentiation of meteoric-sourced snow (with values of δ^{18}O between approximately –15 ‰ to –35 ‰ [44] and sea ice frozen from the ocean water (with second-year ice (SYI) having average δ^{18}O values of –3.1 ‰ and first-year ice with average δ^{18}O values of –0.7 ‰ [40]). This allows us to calculate the percentage of our snowpack originating from meteoric-sourced snow and sublimated sea ice, which we name "ocean-sourced" snow throughout this manuscript. Figure 2a shows our surface snow samples δ^{18}O values have an average of –22.7 ± 6.2 ‰ (n = 35) between January and May 2020. For the same period, the underlying sea ice has δ^{18}O values of –4.5 ± 3.1 ‰ (n = 83). The average snowpack for this season has a mean δ^{18}O of –17.9 ± 8.9 ‰. A simple ratio calculation (1–(–17.9/–22.7) = 0.21 ± 0.01) between these values showed a 21 % enrichment of the δ^{18}O snowpack (with an error of ± 1 % when considering the 0.5‰ measurement accuracy). If our average snow depth is 192 mm ± 158 [41] this corresponds to a snow depth of 40.32 mm (192 mm × 0.21) of ocean-sourced snow. This results in a SWE of 13.44 mm. However, this calculation neglects fractionation processes during metamorphism, which enrich the snow, likely causing a SWE overestimation. Additionally, the error obtained in this calculation through the standard deviation of our isotope profiles (77%) is more significant and is a result of isotopic variability in the snowpack, explained in Appendix B. For this reason, when quantifying the contribution of ocean-sourced snow to the SWE, we focus our analysis on the sublimation rates of an ice surface.

These independent methods have a large variability individually, producing snow depth equivalent values in a similar range. The calculated range of estimated sublimated ice has the ice thickness equivalent of 51–54 mm.

C.3 Influence of TGM on underlying ice

In this manuscript, we found the d-excess value of the underlying sea ice has an average value of 0.2 ‰ (Figure 2b). The extremely negative snow d-excess values of the snow above the interface imply different processes than just a two-component mixture of sea ice and snow. In a recent overview paper, [48] explains how the bottom

boundary of the snow later is more depleted in δ^{18}O than the underlying sea ice surface. However, the surface layer of sea ice itself is also more depleted between FYI and ocean water samples. These isotopic differences together suggest that an additional isotopic exchange between the bottom layer of snow and the sea ice surface layer occurs, and this exchange alters both the isotope composition of the bottom snow and sea ice surface layer samples [48].

During metamorphism, the heavy isotopes remain in the residue, and light isotopes go preferentially to the vapor phase. In the lower snowpack, the isotopic signal we are measuring is a modified sea ice signal instead of a modified snow. Hence, for isotope fractionation, sublimation of the sea ice would start with near-zero delta and d-excess values and not with a "meteoric water" isotope signature with low delta values and high d-excess. As the sea ice is sublimating, we see a heavier isotope signature in the remaining sea ice and lose the lighter isotopes to the snow. This is associated with a decrease in d-excess in the "former" sea ice and an increase in the snow above. It is much easier to generate negative d-excess with sea ice (d-excess, 0‰), than from snow (with a d-excess above 0‰). δ^{18}O values alone are not able to distinguish between a simple two-component mixture and additional disequilibrium fractionation. This is shown only by d-excess values that can be generated by neither of the sources alone.

References

[1] Webster, M., Gerland, S., Holland, M., Hunke, E., Kwok, R., Lecomte, O., Massom, R., Perovich, D., Sturm, M.: Snow in the changing sea-ice systems. Nature Climate Change **8**(11), 946–953 (2018)

[2] Haapala, J., Lensu, M., Dumont, M., Renner, A.H., Granskog, M.A., Gerland, S.: Small-scale horizontal variability of snow, sea-ice thickness and freeboard in the first-year ice region north of svalbard. Annals of Glaciology **54**(62), 261–266 (2013)

[3] Gong, X., Zhang, J., Croft, B., Yang, X., Frey, M.M., Bergner, N., Chang, R.Y.-W., Creamean, J.M., Kuang, C., Martin, R.V., Ranjithkumar, A., Sedlacek, A., Uin, J., Willmes, S., Zawadowicz, M., Pierce, J., Shupe, M., Schmale, J., Wang, J.: Arctic warming by abundant fine sea salt aerosols from blowing snow. Nature Geoscience, 1–7 (2023)

[4] Marelle, L., Thomas, J.L., Ahmed, S., Tuite, K., Stutz, J., Dommergue, A., Simpson, W.R., Frey, M.M., Baladima, F.: Implementation and impacts of surface and blowing snow sources of arctic bromine activation within wrf-chem 4.1. 1. Journal of advances in modeling earth systems **13**(8), 2020–002391 (2021)

[5] Stroeve, J., Notz, D.: Changing state of arctic sea ice across all seasons. Environmental Research Letters **13**(10), 103001 (2018)

[6] Pinzer, B., Schneebeli, M., Kaempfer, T.: Vapor flux and recrystallization during dry snow metamorphism under a steady temperature gradient as observed by

time-lapse micro-tomography. The Cryosphere **6**(5), 1141–1155 (2012)

[7] Sturm, M., Benson, C.S.: Vapor transport, grain growth and depth-hoar development in the subarctic snow. Journal of Glaciology **43**(143), 42–59 (1997)

[8] Ebner, P.P., Steen-Larsen, H.C., Stenni, B., Schneebeli, M., Steinfeld, A.: Experimental observation of transient δ 18 o interaction between snow and advective airflow under various temperature gradient conditions. The Cryosphere **11**(4), 1733–1743 (2017)

[9] Bouvet, L., Calonne, N., Flin, F., Geindreau, C.: Heterogeneous grain growth and vertical mass transfer within a snow layer under temperature gradient. The Cryosphere Discussions **2023**, 1–30 (2023)

[10] Wiese, M.: Time-lapse tomography of mass fluxes and microstructural changes in snow. PhD thesis, ETH Zurich (2017). https://doi.org/10.3929/ethz-b-000213853

[11] Jafari, M., Gouttevin, I., Couttet, M., Wever, N., Michel, A., Sharma, V., Rossmann, L., Maass, N., Nicolaus, M., Lehning, M.: The impact of diffusive water vapor transport on snow profiles in deep and shallow snow covers and on sea ice. Frontiers in Earth Science **8**, 249 (2020)

[12] Dansgaard, W.: Stable isotopes in precipitation. tellus **16**(4), 436–468 (1964)

[13] Beria, H., Larsen, J.R., Ceperley, N.C., Michelon, A., Vennemann, T., Schaefli, B.: Understanding snow hydrological processes through the lens of stable water isotopes. Wiley Interdisciplinary Reviews: Water **5**(6), 1311 (2018)

[14] Madsen, M.V., Steen-Larsen, H.C., Hörhold, M., Box, J., Berben, S.M.P., Capron, E., Faber, A.-K., Hubbard, A., Jensen, M.F., Jones, T., Kipfstuhl, S., Koldtoft, I., Pillar, H.R., Vaughn, B.H., Vladimirova, D., Dahl-Jensen, D.: Evidence of isotopic fractionation during vapor exchange between the atmosphere and the snow surface in greenland. Journal of Geophysical Research: Atmospheres **124**(6), 2932–2945 (2019)

[15] Levasseur, S., Brown, K., Langlois, A., McLennan, D.: Measurement of snow physical properties and stable isotope variations in the canadian sub-arctic and arctic snowpack. Atmosphere-Ocean **59**(3), 137–151 (2021)

[16] Friedman, I.: Isotopic changes during snow metamorphism. Stable isotope geochemistry **3**, 211–221 (1991)

[17] Craig, H., Gordon, L.I.: Deuterium and oxygen 18 variations in the ocean and the marine atmosphere (1965)

[18] Stuart, R.H., Faber, A.K., Wahl, S., Hörhold, M.W., Kipfstuhl, S., Vasskog,

K., Behrens, M., Zuhr, A.M., Steen-Larsen, H.C.: Exploring the role of snow metamorphism on the isotopic composition of the surface snow at eastgrip. The Cryosphere **17**(3), 1185–1204 (2023)

[19] Macfarlane, A.R., Dadic, R., Smith, M.M., Light, B., Nicolaus, M., Henna-Reetta, H., Webster, M., Linhardt, F., Hämmerle, S., Schneebeli, M.: Evolution of the microstructure and reflectance of the surface scattering layer on melting, level arctic sea ice. Elem Sci Anth **11**(1), 00103 (2023)

[20] Domine, F., Sparapani, R., Ianniello, A., Beine, H.: The origin of sea salt in snow on arctic sea ice and in coastal regions. Atmospheric Chemistry and Physics **4**(9/10), 2259–2271 (2004)

[21] Coléou, C., Xu, K., Lesaffre, B., Brzoska, J.-B.: Capillary rise in snow. Hydrological processes **13**(12-13), 1721–1732 (1999)

[22] Barber, D., Ehn, J., Pućko, M., Rysgaard, S., Deming, J., Bowman, J., Papakyriakou, T., Galley, R., Søgaard, D.: Frost flowers on young arctic sea ice: The climatic, chemical, and microbial significance of an emerging ice type. Journal of Geophysical Research: Atmospheres **119**(20), 11–593 (2014)

[23] Rysgaard, S., Søgaard, D.H., Cooper, M., Pucko, M., Lennert, K., Papakyriakou, T.N., Wang, F., Geilfus, N.X., Glud, R.N., Ehn, J., McGinnis, D.F., Attard, K., Sievers, J., Deming, J.W., Barber, D.: Ikaite crystal distribution in winter sea ice and implications for co_2 system dynamics. The Cryosphere **7**(2), 707–718 (2013). https://doi.org/10.5194/tc-7-707-2013

[24] Lapere, R., Thomas, J.L., Marelle, L., Ekman, A.M., Frey, M.M., Lund, M.T., Makkonen, R., Ranjithkumar, A., Salter, M.E., Samset, B.H., Schulz, M., Sogacheva, L., Yang, X., Zieger, P.: The representation of sea salt aerosols and their role in polar climate within cmip6. Journal of Geophysical Research: Atmospheres **128**(6), 2022–038235 (2023)

[25] Pratt, K.A., Custard, K.D., Shepson, P.B., Douglas, T.A., Pöhler, D., General, S., Zielcke, J., Simpson, W.R., Platt, U., Tanner, D.J., Gregory Huey, L., Carlsen, M., Stirm, B.: Photochemical production of molecular bromine in arctic surface snowpacks. Nature Geoscience **6**(5), 351–356 (2013)

[26] Baccarini, A., Karlsson, L., Dommen, J., Duplessis, P., Vüllers, J., Brooks, I.M., Saiz-Lopez, A., Salter, M., Tjernström, M., Baltensperger, U., Zieger, P., Schmale, J.: Frequent new particle formation over the high arctic pack ice by enhanced iodine emissions. Nature Communications **11**(1), 4924 (2020)

[27] Benavent, N., Mahajan, A.S., Li, Q., Cuevas, C.A., Schmale, J., Angot, H., Jokinen, T., Quéléver, L.L.J., Blechschmidt, A.-M., Zilker, B., Richter, A., Serna, J.A., Garcia-Nieto, D., Fernandez, R.P., Skov, H., Dumitrascu, A., Simões Pereira, P., Abrahamsson, K., Bucci, S., Duetsch, M., Stohl, A., Beck, I., Laurila, T.,

Blomquist, B., Howard, D., Archer, S.D., Bariteau, L., Helmig, D., Hueber, J., Jacobi, H.-W., Posman, K., Dada, L., Daellenbach, K.R., Saiz-Lopez, A.: Substantial contribution of iodine to arctic ozone destruction. Nature Geoscience (Online) **15**(10) (2022). https://doi.org/10.1038/s41561-022-01018-w

[28] Flanner, M., Liu, X., Zhou, C., Penner, J.E., Jiao, C.: Enhanced solar energy absorption by internally-mixed black carbon in snow grains. Atmospheric Chemistry and Physics **12**(10), 4699–4721 (2012)

[29] Arndt, S., Haas, C., Meyer, H., Peeken, I., Krumpen, T.: Recent observations of superimposed ice and snow ice on sea ice in the northwestern weddell sea. The Cryosphere **15**(9), 4165–4178 (2021)

[30] Macfarlane, A.R., Löwe, H., Gimenes, L., Wagner, D.N., Dadic, R., Ottersberg, R., Hämmerle, S., Schneebeli, M.: Thermal conductivity of snow on arctic sea ice. EGUsphere **2023**, 1–22 (2023). https://doi.org/10.5194/egusphere-2023-83

[31] Wagner, D.N., Shupe, M.D., Cox, C., Persson, O.G., Uttal, T., Frey, M.M., Kirchgaessner, A., Schneebeli, M., Jaggi, M., Macfarlane, A.R., Itkin, P., Arndt, S., Hendricks, S., Krampe, D., Nicolaus, M., Ricker, R., Regnery, J., Kolabutin, N., Shimanshuck, E., Oggier, M., Raphael, I., Stroeve, J., Lehning, M.: Snowfall and snow accumulation during the mosaic winter and spring seasons. The Cryosphere **16**(6), 2373–2402 (2022). https://doi.org/10.5194/tc-16-2373-2022

[32] Webster, M., DuVivier, A., Holland, M., Bailey, D.: Snow on arctic sea ice in a warming climate as simulated in cesm. Journal of Geophysical Research: Oceans **126**(1), 2020–016308 (2021)

[33] Diebold, F.X., Rudebusch, G.D., Göbel, M., Coulombe, P.G., Zhang, B.: When will arctic sea ice disappear? projections of area, extent, thickness, and volume. Journal of Econometrics **236**(2), 105479 (2023)

[34] Nicolaus, M., Perovich, D.K., Spreen, G., Granskog, M.A., von Albedyll, L., Angelopoulos, M., Anhaus, P., Arndt, S., Belter, H.J., Bessonov, V., Birnbaum, G., Brauchle, J., Calmer, R., Cardellach, E., Cheng, B., Clemens-Sewall, D., Dadic, R., Damm, E., de Boer, G., Demir, O., Dethloff, K., Divine, D.V., Fong, A.A., Fons, S., Frey, M.M., Fuchs, N., Gabarró, C., Gerland, S., Goessling, H.F., Gradinger, R., Haapala, J., Haas, C., Hamilton, J., Hannula, H.-R., Hendricks, S., Herber, A., Heuzé, C., Hoppmann, M., Høyland, K.V., Huntemann, M., Hutchings, J.K., Hwang, B., Itkin, P., Jacobi, H.-W., Jaggi, M., Jutila, A., Kaleschke, L., Katlein, C., Kolabutin, N., Krampe, D., Kristensen, S.S., Krumpen, T., Kurtz, N., Lampert, A., Lange, B.A., Lei, R., Light, B., Linhardt, F., Liston, G.E., Loose, B., Macfarlane, A.R., Mahmud, M., Matero, I.O., Maus, S., Morgenstern, A., Naderpour, R., Nandan, V., Niubom, A., Oggier, M., Oppelt, N., Pätzold, F., Perron, C., Petrovsky, T., Pirazzini, R., Polashenski, C., Rabe, B., Raphael, I.A., Regnery, J., Rex, M., Ricker, R., Riemann-Campe, K., Rinke, A., Rohde, J., Salganik, E., Scharien, R.K., Schiller, M., Schneebeli, M., Semmling, M., Shimanchuk, E.,

Shupe, M.D., Smith, M.M., Smolyanitsky, V., Sokolov, V., Stanton, T., Stroeve, J., Thielke, L., Timofeeva, A., Tonboe, R.T., Tavri, A., Tsamados, M., Wagner, D.N., Watkins, D., Webster, M., Wendisch, M.: Overview of the MOSAiC expedition: Snow and sea ice (2022). https://doi.org/10.1525/elementa.2021.000046. https://doi.org/10.1525/elementa.2021.000046

[35] Macfarlane, A.R., Schneebeli, M., Dadic, R., Wagner, D.N., Arndt, S., Clemens-Sewall, D., Hämmerle, S., Hannula, H.-R., Jaggi, M., Kolabutin, N., Krampe, D., Lehning, M., Matero, I., Nicolaus, M., Oggier, M., Pirazzini, R., Polashenski, C., Raphael, I., Regnery, J., Shimanchuck, E., Smith, M.M., Tavri, A.: Snowpit raw data collected during the MOSAiC expedition. PANGAEA (2021). https://doi.org/10.1594/PANGAEA.935934. https://doi.org/10.1594/PANGAEA.935934

[36] Macfarlane, A.R., Schneebeli, M., Dadic, R., Tavri, A., Immerz, A., Polashenski, C., Krampe, D., Clemens-Sewall, D., Wagner, D.N., Perovich, D.K., Henna-Reetta, H., Raphael, I., Matero, I., Regnery, J., Smith, M.M., Nicolaus, M., Jaggi, M., Oggier, M., Webster, M.A., Lehning, M., Kolabutin, N., Itkin, P., Naderpour, R., Pirazzini, R., Hämmerle, S., Arndt, S., Fons, S.: Author Correction: A Database of Snow on Sea Ice in the Central Arctic Collected during the MOSAiC expedition. Scientific Data **10**(1), 500 (2023). https://doi.org/10.1038/s41597-023-02413-7

[37] Macfarlane, A.R., Schneebeli, M., Wagner, D.N., Dadic, R., Jaggi, M., Hämmerle, S.: MicroCT density and specific surface area snowpit profiles during the MOSAiC expedition. PANGAEA (2022). https://doi.org/10.1594/PANGAEA.952794. In: Macfarlane, AR et al. (2021): Snowpit raw data collected during the MOSAiC expedition. PANGAEA, https://doi.org/10.1594/PANGAEA.935934. https://doi.pangaea.de/10.1594/PANGAEA.952794

[38] Macfarlane, A.R., Schneebeli, M., Dadic, R., Wagner, D.N., Arndt, S., Clemens-Sewall, D., Hämmerle, S., Hannula, H.-R., Jaggi, M., Kolabutin, N., Krampe, D., Lehning, M., Matero, I., Nicolaus, M., Oggier, M., Pirazzini, R., Polashenski, C., Raphael, I., Regnery, J., Shimanchuck, E., Smith, M.M., Tavri, A., Mellat, M., Meyer, H., Werner, M., Brunello, C.F.: Snowpit stable isotope profiles during the MOSAiC expedition. PANGAEA (2022). https://doi.org/10.1594/PANGAEA.952556. In: Macfarlane, AR et al. (2021): Snowpit raw data collected during the MOSAiC expedition. PANGAEA, https://doi.org/10.1594/PANGAEA.935934. https://doi.pangaea.de/10.1594/PANGAEA.952556

[39] Macfarlane, A.R., Schneebeli, M., Dadic, R., Wagner, D.N., Arndt, S., Clemens-Sewall, D., Hämmerle, S., Hannula, H.-R., Jaggi, M., Kolabutin, N., Krampe, D., Lehning, M., Matero, I., Nicolaus, M., Oggier, M., Pirazzini, R., Polashenski, C., Raphael, I., Regnery, J., Shimanchuck, E., Smith, M.M., Tavri, A.: Snowpit salinity profiles during the MOSAiC expedition. PANGAEA (2022). https://doi.org/10.1594/PANGAEA.946807. In: Macfarlane, AR et al.

(2021): Snowpit raw data collected during the MOSAiC expedition. PANGAEA, https://doi.org/10.1594/PANGAEA.935934. https://doi.pangaea.de/10.1594/PANGAEA.946807

[40] Mellat, M., Meyer, H., Brunello, C.F., Arndt, S., Macfarlane, A.R., Schneebeli, M., Hörhold, M., Werner, M., Weiner, M., Marent, A.: Stable water isotopes of snow during MOSAiC expedition. PANGAEA (2022). https://doi.org/10.1594/PANGAEA.948511. https://doi.org/10.1594/PANGAEA.948511

[41] Macfarlane, A.R., Schneebeli, M., Dadic, R., Wagner, D.N., Arndt, S., Clemens-Sewall, D., Hämmerle, S., Hannula, H.-R., Jaggi, M., Kolabutin, N., Krampe, D., Lehning, M., Matero, I., Nicolaus, M., Oggier, M., Pirazzini, R., Polashenski, C., Raphael, I., Regnery, J., Shimanchuck, E., Smith, M.M., Tavri, A.: Snowpit height measurements during the MOSAiC expedition. PANGAEA (2022). https://doi.org/10.1594/PANGAEA.940215. In: Macfarlane, AR et al. (2021): Snowpit raw data collected during the MOSAiC expedition. PANGAEA, https://doi.org/10.1594/PANGAEA.935934. https://doi.org/10.1594/PANGAEA.940215

[42] Dadic, R., Schneebeli, M., Bertler, N.A., Schwikowski, M., Matzl, M.: Extreme snow metamorphism in the allan hills, antarctica, as an analogue for glacial conditions with implications for stable isotope composition. Journal of Glaciology **61**(230), 1171–1182 (2015)

[43] Steen-Larsen, H.C., Masson-Delmotte, V., Hirabayashi, M., Winkler, R., Satow, K., Prié, F., Bayou, N., Brun, E., Cuffey, K.M., Dahl-Jensen, D., Dumont, M., Guillevic, M., Kipfstuhl, S., Landais, A., Popp, T., Risi, C., Steffen, K., Stenni, B., Sveinbjörnsdottír, A.E.: What controls the isotopic composition of greenland surface snow? Climate of the Past **10**(1), 377–392 (2014). https://doi.org/10.5194/cp-10-377-2014

[44] Ala-aho, P., Welker, J.M., Bailey, H., Højlund Pedersen, S., Kopec, B., Klein, E., Mellat, M., Mustonen, K.-R., Noor, K., Marttila, H.: Arctic snow isotope hydrology: A comparative snow-water vapor study. Atmosphere **12**(2) (2021). https://doi.org/10.3390/atmos12020150

[45] Granskog, M.A., Rösel, A., Dodd, P.A., Divine, D., Gerland, S., Martma, T., Leng, M.J.: Snow contribution to first-year and second-year arctic sea ice mass balance north of svalbard. Journal of Geophysical Research: Oceans **122**(3), 2539–2549 (2017)

[46] Pauling, A.G., Bitz, C.M.: Arctic sea ice response to flooding of the snow layer in future warming scenarios. Earth's Future **9**(10), 2021–002136 (2021)

[47] Macfarlane, A.R.: Influences of snow microstructure on the arctic sea ice energy budget. PhD thesis, ETH Zurich (2023)

[48] Mellat, M., Brunello, C., Werner, M., Bauch, D., Damm, E., Angelopoulos, M., Nomura, D., Welker, J., Schneebeli, M., Granskog, M., Hoerhold, M., Macfarlane, A., Arndt, S., Meyer, H.: Isotopic signatures of snow, sea ice, and surface seawater in the central arctic ocean during the mosaic expedition. Elementa: Science of the Anthropocene (In review)